

Crafting Query-Aware Selective Attention for Single Image Super-Resolution

Junyoung Kim¹, Youngrok Kim², Siyeol Jung³, Donghyun Min⁴
¹POSTECH, ²Kyunghee University, ³UNIST, ⁴Sogang University
junyoungkim@postech.ac.kr, faller825@khu.ac.kr,
siyeol@unist.ac.kr, mdh38112@sogang.ac.kr

Abstract

Single Image Super-Resolution (SISR) reconstructs high-resolution images from low-resolution inputs, enhancing image details. While Vision Transformer (ViT)-based models improve SISR by capturing long-range dependencies, they suffer from quadratic computational costs or employ selective attention mechanisms that do not explicitly focus on query-relevant regions. Despite these advancements, prior work has overlooked how selective attention mechanisms should be effectively designed for SISR. We propose SSCAN, which dynamically selects the most relevant key-value windows based on query similarity, ensuring focused feature extraction while maintaining efficiency. In contrast to prior approaches that apply attention globally or heuristically, our method introduces a query-aware window selection strategy that better aligns attention computation with important image regions. By incorporating fixed-sized windows, SSCAN reduces memory usage and enforces linear token-to-token complexity, making it scalable for large images. Our experiments demonstrate that SSCAN outperforms existing attention-based SISR methods, achieving up to 0.14 dB PSNR improvement on urban datasets, guaranteeing both computational efficiency and reconstruction quality in SISR.

1. Introduction

Single Image Super-Resolution (SISR) aims to reconstruct high-resolution (HR) images from low-resolution (LR) inputs, enhancing image quality and detail preservation in various applications. SISR is widely used in fields such as satellite imagery and digital photography, where high-resolution outputs are crucial for accurate interpretation and analysis [10, 16, 22, 26, 31, 40]. Even for large-scale applications such as remote sensing and medical imaging, precise and detailed enhancement is necessary to extract meaningful information [37, 45, 49]. However, deploying SISR in real-world scenarios requires a balance between performance and efficiency, as high-resolution processing must be

lightweight for practical use in real-time systems [5, 17].

For instance, modern surveillance systems and smartphones incorporate on-device SISR processing under constrained memory environments, ensuring real-time performance [1, 7]. Similarly, social media platforms such as Instagram and Snapchat use real-time super-resolution to enhance image quality while maintaining computational efficiency on mobile devices [24]. These examples highlight the necessity of designing SISR models that achieve high-quality image restoration without excessive computational cost.

Recent deep learning-based SISR methods have significantly improved performance. Convolutional Neural Networks (CNNs) have been widely adopted due to their ability to extract local image features effectively [12, 13, 23, 29]. However, CNNs struggle to model long-range dependency due to their inherent locality inductive bias [15], making them less suitable for realistic human-interactive environments. To address this limitation, Transformer-based architectures incorporating self-attention mechanisms have been developed [42]. These models dynamically weigh the importance of different regions in the input sequence, enabling better global feature learning [8, 9, 15, 28, 36, 42]. Despite their advantages, a key challenge with typical transformer-based SISR techniques is their high computational complexity. The typical self-attention mechanisms calculate token affinity across all spatial locations, causing computational costs to grow quadratically with image size. This limits their deployment in resource-constrained environments [9].

To mitigate these computational challenges, recent models have explored various types of selective attention mechanisms as an alternative [14, 41, 44, 53, 55]. For example, SwinIR adopts a window-based self-attention approach [32], restricting computations to non-overlapping local windows and significantly reducing complexity. Similarly, grouped attention methods [35] aims to enhance efficiency by selectively processing image regions. Although these approaches improve efficiency, they still rely on fixed partitioning rather than dynamically selecting relevant re-

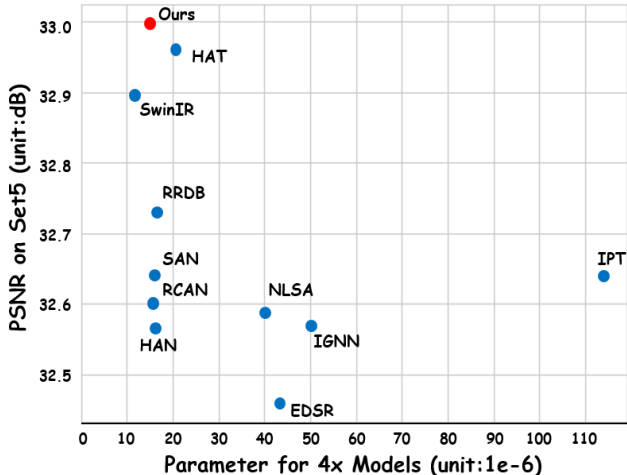


Figure 1. The comparisons of recent transformer-based SR models in terms of PSNR and parameters on Urban100 dataset. Our model (SSCAN) outperforms the SOTA models ($\times 4$) by up to 0.14dB in PSNR.

gions, limiting their ability to adapt to varying semantic importance. Consequently, they struggle to fully capture the contextual relevance of image regions.

In this work, we try to bridge this gap by proposing **SSCAN** (Super-resolution using **S**elective and **C**ontext-aware **A**ttention-based **N**etwork). SSCAN dynamically selects the most relevant regions based on query-key similarity tailored for super-resolution. This context-aware selective attention ensures that only the most informative image regions contribute to reconstruction, reducing computational complexity even for large-scale images while enhancing reconstruction fidelity. Our main contributions are the following:

1. We proposed fine-grained context-aware attention (FGCA), selective top-k attention for SISR that dynamically attends to the most relevant semantic regions, regardless of image size.
2. SSCAN maintains the same architecture and hyperparameters as SwinIR, with the only modification being the integration of our FGCA block into the attention module.
3. SSCAN significantly outperforms SwinIR, achieving up to **0.14dB** improvement over the state-of-the-art selective attention-based SISR model (Refer to Figure 1).
4. Despite its performance, SSCAN maintains computational efficiency, not exceeding the quadratic overhead increase observed in the recent selective attention.

2. Related Work

2.1. Image Super-resolution

Image super-resolution (SR) is designed to enhance the visual quality and details of low-resolution (LR) images by converting them into their high-resolution (HR) equiv-

alents [4]. This task is fundamentally an ill-posed inverse problem, where multiple HR solutions could theoretically exist for a single LR input. This complexity increases with the scaling factor, emphasizing the need for sophisticated approaches that can infer accurate HR images. Traditionally, SR techniques have modeled the relationship between LR and HR images through various degradation functions. Typically, these functions include bicubic interpolation, which is often augmented with noise and other custom kernels to mimic real-world conditions. The selection of a particular degradation function significantly influences the performance of SR models, as it dictates the initial assumptions about how the LR image degrades.

Over the last few decades, deep learning has revolutionized SR by learning from extensive prior data [12, 13, 21, 23, 29]. Beginning with models such as SRCNN [12] that utilized deep convolutional neural networks, the field has experienced a notable shift towards increasingly complex architectures. These are designed to more effectively capture and reconstruct fine image details. Adversarial learning further advanced the field by emphasizing perceptual quality, thereby enhancing the realism of upsampled images [25, 38, 45].

2.2. Selective Attention based Transformers in Super-resolution

The Transformer architecture [42], originally developed for natural language processing, has been successfully adapted to vision tasks, including super-resolution (SISR). The Vision Transformer (ViT) [15] applies self-attention to image patches, treating each as a token and modeling their global interactions. While this approach effectively captures long-range dependencies, it generates low-resolution feature maps that compromise the capture of fine-grained spatial details. Additionally, its global attention mechanism scales quadratically with input size, resulting in significant computational overhead.

To address these issues, selective attention-based SISR models have been introduced to improve computational efficiency while preserving or enhancing key spatial details. The selective attention methods dynamically determine which spatial regions or feature representations to attend to, rather than processing all token pairs indiscriminately. This general paradigm can be further categorized into several key branches: local, axial, and dynamic attention, each offering distinct advantages in balancing efficiency and feature expressiveness.

Local attention (regionally constrained selective attention). Local attention is one of the earliest forms of selective attention, where models restrict attention computations to localized regions to reduce complexity while preserving fine details. Swin Transformer [32] employs a hierarchical model using window-based self-attention, lim-

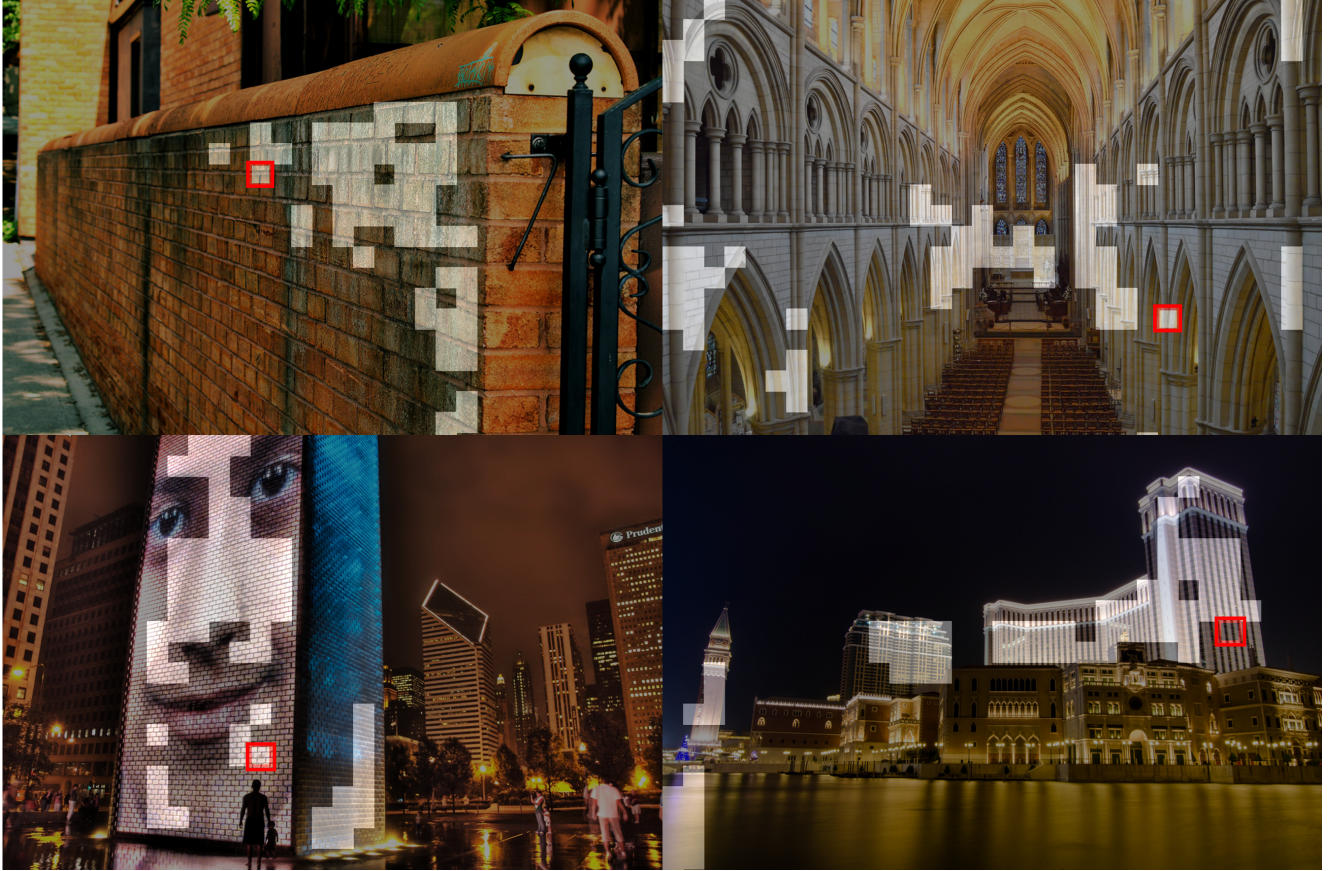


Figure 2. Visualization of our proposed Fine-Grained Context-Aware Attention (FGCA) on Urban100 dataset: Red boxes indicate query regions, while white boxes denote corresponding key regions.

iting attention operations to non-overlapping local windows. This method reduces computational costs significantly while maintaining spatial precision. Moreover, shifted window mechanisms [36, 24] help extend contextual understanding by allowing gradual information exchange between neighboring regions. While this class of attention [9, 50] can dramatically reduce the computational burden and improve the model’s capacity to incorporate detailed spatial information across various scales.

Axial attention (structured selective attention). Axial attention builds upon local attention by further constraining self-attention operations along specific spatial axes (rows and columns) rather than over entire feature maps. For example, MaxVit [41] introduces an axial-based attention mechanism that processes images in structured blocks and grids, enabling a balance between local detail capture and global contextual understanding. Although this method offers computational efficiency compared to fully global attention, its structured nature may impose rigid constraints on adaptability, making it less effective in handling non-uniform feature distributions across images.

Dynamic attention (adaptive selective attention). Dy-

amic attention, also called adaptive selective attention, provides a more flexible approach than conventional selective attention mechanisms. Instead of relying on predefined local or axial partitions, dynamic attention allows adaptively adjusting their attention structures based on input characteristics. Recent studies [55] have integrated dynamic attention mechanisms into vision transformers for selectively refining which regions contribute most to feature representation. This adaptability significantly improves both computational efficiency and the ability to capture complex spatial structures [39, 47, 48]. However, existing dynamic attention mechanisms have been primarily designed for general vision tasks. In the context of SISR, a specialized design is required to guarantee fine texture restoration, edge preservation, and repetitive pattern processing.

3. Proposed Method

Our study establishes and provides acceptable architecture design that adopts query-aware and adaptive selective attention for SISR. In this section, we present an overview of our SSCAN model, as illustrated in Figure 3. We then provide a detailed description of our fine-grained context-aware atten-

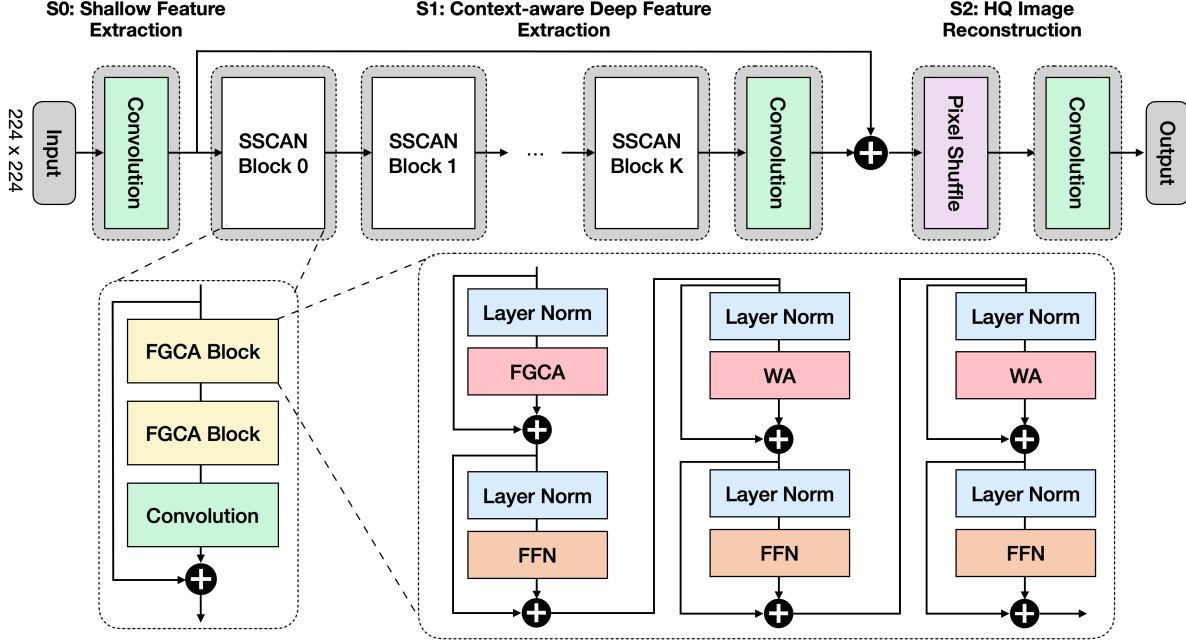


Figure 3. The overall architecture of SSCAN model and the composition of SSCAN block. Each SSCAN block has two FGCA blocks in this illustration.

tion (FGCA) for SISR and introduce core component block, namely the Residual SSCAN Block (SSCAN block).

3.1. Network architecture

As shown in Figure 3, SSCAN consists of 3-stages. For a low-resolution image $I_{LR} \in \mathbb{R}^{H \times W \times C_{in}}$, where H, W, C_{in} denote the height, width, and channels of the input image, the feature map is extracted through a 3×3 convolution layer H_{SFE} in the shallow feature extraction step.

$$F_0 = H_{SFE}(I_{LR}), \quad (1)$$

The subscript zero in F_0 denotes the feature obtained after the shallow feature extraction stage. We stacked multiple SSCAN blocks in the deep feature extraction part to extract deeper features.

$$F_{DF} = H_{DF}(F_0), \quad (2)$$

where $F_{DF} \in \mathbb{R}^{H \times W \times C}$ is the extracted deep feature and $H_{DF}(\cdot)$ is the deep feature extraction module.

After deep feature extraction, we use the residual path to reflect the features extracted by shallow feature extraction. H_{Conv} is the last convolution layer in the deep feature extraction process and K is the number of SCNB blocks.

$$F_{DF} = H_{Conv}(F_K) + F_0, \quad (3)$$

In the reconstruction part, we reconstruct the features that have passed through the model into high resolution fea-

tures using the reconstruction module consisting of the pixel shuffle function.

$$I_{SR} = H_{rec}(F_{DF}), \quad (4)$$

where $I_{SR} \in \mathbb{R}^{H \times W \times C_{in}}$ is reconstructed super-resolution image, and $H_{rec}(\cdot)$ is reconstruction function to upscale I_{SR} to proposed scale.

3.2. Design of Residual SSCAN Block

Our model consists of multiple stacks of SSCAN block. It contains L fine-grained context-aware attention (FGCA) blocks and a single $\text{Conv}(\cdot)$ layer for feature transition at the last position. Given the feature $F_{i,0}$ of input, we can extract deep features using L layers of FGCA.

$$F_{i,j} = H_{i,j}(F_{i,j-1}) + F_{i,0}, \quad (5)$$

where $H_{i,j}(\cdot)$ is the j -th FGCA in the i -th FGCA. FGCA block consists of FGCA to extract context-aware features, window attention (WA), and shifted window attention (SWA) to extract local features. This structure is designed to capture both local features and context-aware features adaptive to the query. Also, We positioned the FGCA layer ahead of the WA layer to capture global and context-aware features first to prevent potential bias between local and global features. This led to an increase in SISR performance, as detailed in Section 4.5.

3.3. Fine-grained Context-aware Attention (FGCA)

Inspired by [55], our strategy of FGCA is to find the similarity between the query and key-value and perform attention using only the top-k similar key-value windows through the projection, routing, and token-to-token attention steps. In the projection step, an input image feature $\mathbf{X} \in \mathbb{R}^{H \times W \times C}$ are divided into $\mathbf{X}^r \in \mathbb{R}^{M^2 \times \frac{HW}{M^2} \times C}$ regions such that each region has $M \times M$ feature vectors, where M is the window size. For the partitioned region, we can drive query, key and value, $\mathbf{Q}, \mathbf{K}, \mathbf{V} \in \mathbb{R}^{M^2 \times \frac{HW}{M^2} \times C}$ by using linear projections. In the routing step, fine-grained context-aware attention gathers the top-k similar key-value windows. The relevant windows can be identified by using Equation 6, which computes the relevance between the two regions.

$$\mathbf{A}^r = \mathbf{Q}^r (\mathbf{K}^r)^T \quad (6)$$

where $\mathbf{Q}^r, \mathbf{K}^r \in \mathbb{R}^{M^2 \times C}$ denote that the query and key region. Entries in the adjacency matrix \mathbf{A}^r indicate how semantically related the query and key are. Only the top-k image regions with the highest similarity are routed to the token-to-token attention step, while the rest row-wise are pruned. In the token-to-token attention step, the actual attention operation is performed using Equation 7 on each query with the top-k selected key-value pairs.

$$\mathbf{O} = \text{softmax} \left(\frac{\mathbf{Q}\mathbf{K}^T}{\sqrt{d}} \right) \mathbf{V} \quad (7)$$

where the d denotes the hidden dimensions of \mathbf{Q} and \mathbf{K} vectors.

In the previous works [55], the window size is variable, causing inconsistencies in image interpretation between the training and inference phases. This discrepancy leads to mismatches in the amount of information processed, potentially driving the model towards a suboptimal solution. On the other hand, our proposed methods maintain a consistent window size across both training and inference. It ensures stability in information processing and ensures that the intended training content is accurately reflected during inference.

Furthermore, this is expected to be more efficient in terms of computation and memory footprint as the input size increases. According to Equation 8 and Equation 9, our attention mechanism is more advantageous than previous methods [55], reducing the substantial load of computation during the token-to-token attention from quadratic to linear, preventing computational overload as image size increases.

$$FLOPS_{Prev} = \overbrace{2(S^2)^2 C}^{\text{Routing}} + \underbrace{2k(HW)^2 S^2 C}_{\text{Attention}}, \quad (8)$$

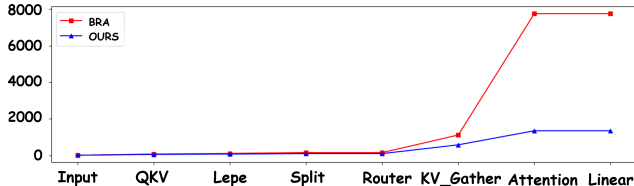


Figure 4. Comparison of memory consumption between Bi-Former’s attention (BRA) and our fine-grained context-aware attention during calculating attention score.

$$FLOPS_{Ours} = \overbrace{2(HW)^2 M^4 C}^{\text{Routing}} + \underbrace{2kM^2(HW)C}_{\text{Attention}}, \quad (9)$$

where k is top-k parameters, S^2 is the variable window size proposed in [55], and M^2 denotes SSCAN’s fixed window size.

For large images (H and $W \gg M$), the relationship $S^2 \gg M^2$ holds, leading to significantly higher memory usage for previous works compared to SSCAN. The experimental results shown in Figure 4 empirically validate this theoretical analysis. In Table 4, the result supports the theoretical advantages of fine-grained context-aware attention. In particular, the better performance of smaller window sizes (4×4) on the Urban100 dataset demonstrates the effectiveness of fine-grained context-aware attention in recognizing repetitive patterns. Table 3 shows that capturing global context (fine-grained context-aware attention) first and refining local details (WA) is more effective for SISR, which aligns with our theoretical framework. Lastly, Figure 5 demonstrates that fine-grained context-aware attention can more accurately restore repetitive patterns and fine details, due to its ability to recognize semantic similarities.

4. Experiments

4.1. Experimental Setups

We employed the identical model architecture and hyperparameters as Light-SwinIR [28, 52] to evaluate the comparative efficacy of window attention versus our proposed fine-grained context-aware attention. Our setup includes two FGCA blocks and four SSCAN blocks. The window sizes are set to 8×8 and 60 embedding dimensions. We used Adam optimizer and trained for $500k$ iterations on the DIV2K [2] datasets with a batch size of 64 and L1 loss as the loss function.

During training, we captured information using 32 top-k, increasing to 64 top-k during inference to include more context-aware information. To improve generalizability, we applied data augmentation techniques including random horizontal flip, random vertical flip, rotation, and random crop.

Table 1. Quantitative comparison with state-of-the-art methods achieved for $\times 2/3/4$ SR. The best and second best performances are in red and blue.

Model	#PARAMS	Scale	Set5		Set14		BSD100		Urban100	
			PSNR	SSIM	PSNR	SSIM	PSNR	SSIM	PSNR	SSIM
CARN [3]	1592K	$\times 2$	37.76	0.959	33.52	0.9166	32.09	0.8978	31.92	0.9256
IMDN [20]	694K		38	0.9605	33.63	0.9177	32.19	0.8996	32.17	0.9283
AWSRN-M [43]	1063K		38.04	0.9605	33.66	0.9181	32.21	0.9000	32.23	0.9294
LAPAR-A [27]	548K		38.01	0.9605	33.62	0.9183	32.19	0.8999	32.10	0.9283
RFDN [30]	534K		38.05	0.9606	33.68	0.9184	32.16	0.8994	32.12	0.9278
LatticeNet [33]	756K		38.06	0.9607	33.70	0.9187	32.20	0.8999	32.25	0.9288
AAF-L [46]	1363K		38.09	0.9607	33.78	0.9192	32.23	0.9002	32.46	0.9313
A-CubeNet [18]	1376K		38.12	0.9609	33.73	0.9191	32.26	0.9007	32.39	0.9308
Swin-Light [28]	878K		38.14	0.9611	33.86	0.9206	32.31	0.9012	32.76	0.934
ELAN-Light [54]	582K		38.17	0.9611	33.94	0.9207	32.30	0.9012	32.76	0.934
SSCAN (Ours)	911K		38.27	0.9615	33.93	0.9211	32.33	0.9016	32.71	0.9337
CARN [3]	1592K	$\times 3$	34.29	0.9255	30.29	0.8407	29.06	0.8034	28.06	0.8493
IMDN [20]	703K		34.36	0.827	30.32	0.8417	29.09	0.8046	28.17	0.8519
AWSRN-M [43]	1143K		34.42	0.9275	30.32	0.8419	29.13	0.8059	28.26	0.8545
LAPAR-A [27]	544K		34.36	0.9267	30.34	0.8421	29.11	0.8054	28.15	0.8523
RFDN [30]	541K		34.41	0.9273	30.34	0.842	29.09	0.805	28.21	0.8525
LatticeNet [33]	765K		34.40	0.9272	30.32	0.8416	29.10	0.8049	28.19	0.8513
AAF-L [46]	1367K		34.53	0.9281	30.45	0.8441	29.17	0.8068	28.38	0.8568
A-CubeNet [18]	1561K		34.54	0.9283	30.41	0.8436	29.14	0.8062	28.40	0.8574
Swin-Light [28]	886K		34.62	0.9289	30.54	0.8463	29.20	0.8082	28.66	0.8624
ELAN-Light [54]	590K		34.64	0.9288	30.55	0.8463	29.21	0.8081	28.69	0.8624
SSCAN (Ours)	919K		34.62	0.9292	30.61	0.8466	29.25	0.8095	28.74	0.8638
CARN [3]	1592K	$\times 4$	32.13	0.8937	28.60	0.7806	27.58	0.7349	26.07	0.7837
IMDN [20]	715K		32.21	0.8948	28.58	0.7811	27.56	0.7353	26.04	0.7838
AWSRN-M [43]	1254K		32.21	0.8954	28.65	0.7832	27.60	0.7368	26.15	0.7884
LAPAR-A [27]	659K		32.15	0.8944	28.61	0.7818	27.61	0.7366	26.14	0.7871
RFDN [30]	550K		32.24	0.8952	28.61	0.7819	27.57	0.7360	26.11	0.7858
LatticeNet [33]	777K		32.30	0.8962	28.68	0.783	27.62	0.7367	26.25	0.7873
AAF-L [46]	1374K		32.32	0.8964	28.67	0.7839	27.62	0.7379	26.32	0.7931
A-CubeNet [18]	1524K		32.32	0.8969	28.72	0.7847	27.65	0.7382	26.27	0.7913
Swin-Light [28]	897K		32.44	0.8976	28.77	0.7858	27.69	0.7406	26.47	0.7980
ELAN-Light [54]	601K		32.43	0.8975	28.78	0.7858	27.69	0.7406	26.54	0.7982
SSCAN (Ours)	931K		32.58	0.8991	28.88	0.7878	27.74	0.7422	26.65	0.8021

4.2. Datasets

We train with DIV2K [2] datasets. This dataset includes 800 images for training images. We conduct performance evaluation with four standard benchmark datasets, Set5 [6], Set14 [51], BSD100 [34] and Urban100 [19] in terms of PSNR and SSIM metrics.

4.3. Quantitative Comparison with Existing Super-resolution Models

In Table 1, we compare our model with the following super-resolution methods that can operate in resource-constrained environments, demonstrating state-of-the-art performance: CARN [3], IMDN [20], AWSRN-M [43], LAPAR-A [27],

RFDN [30], LatticeNet [33], AAF-L [46], A-CubeNet [18], SwinIR-light [28] and ELAN-light [54]. Note that Swin-Light is a lightweight version of SwinIR [28] enhancing to capture local information and ELAN-Light [54] introduce efficient long-range shared attention mechanism using two shift-convolution network. Our method achieves a significant performance improvement while maintaining a similar number of parameters in previous work. Moreover, at a scale factor of $\times 2$ and $\times 3$, we can see that there are the second-best performance achievements for some datasets. In contrast, at a scale factor of $\times 4$, our SSCAN achieves the best results with surprising improvements on all benchmark datasets. This is because even if the model routes the

Table 2. An ablation study of the effectiveness of top-k during the inference phase.

Top-k	Set5	Set14	BSD100	Urban100
	PSNR / SSIM	PSNR / SSIM	PSNR / SSIM	PSNR / SSIM
32	32.565 / 0.8991	28.852 / 0.7875	27.722 / 0.7421	26.557 / 0.7997
48	32.576 / 0.8992	28.869 / 0.7877	27.731 / 0.7422	26.618 / 0.8013
64	32.576 / 0.8991	28.879 / 0.7878	27.735 / 0.7422	26.652 / 0.8021

same top-k key-value windows for all scale factors, the input image size is the largest at scale $\times 2$, followed by $\times 3$ and $\times 4$, so the ratio of the amount of information ($M \times k$) to the image size is smallest for $\times 2$ and largest for $\times 4$. Accordingly, our SSCAN performs in terms of PSNR with $-0.05\text{dB} \sim 0.1\text{dB}$ for $\times 2$, whereas $0.05\text{dB} \sim 0.14\text{dB}$ for $\times 4$. Our SSCAN is ideally suitable for reconstructing images from small image sizes to larger ones with higher upscaling.

4.4. Analysis of Memory Usage

We analyze the memory usage of each component in the Bi-Routing Attention (BRA) mechanism of the BiFormer [55], as depicted in Figure 4. While BRA surpasses state-of-the-art in numerous downstream tasks, it exhibits substantial memory consumption. This is primarily due to the storage requirements for the $Q \times K$ computation results and subsequent softmax operations, as illustrated in Figure 4. These intermediate results are stored in DRAM, leading to increased memory access overhead, which in turn causes system latency. Such high memory demands are unsuitable for resource-constrained environments. To alleviate this complexity, adopting a fixed window size approach can be effective. When the input image size exceeds $(M \times S, M \times S)$, processes larger query, key, and value regions than (M, M) . In these scenarios, storing computation results consumes more memory compared to fine-grained context-aware attention, which consistently operates on $M \times M$ window, irrespective of input size. As a result, fine-grained context-aware attention offers a memory usage advantage for super-resolving large images in resource-limited settings. Furthermore, FlashAttention [11] effectively addresses these problems by partitioning the query, key, and value matrices into blocks and computing them entirely within on-chip SRAM. By applying 1) fixed window size and 2) FlashAttention, our fine-grained context-aware attention can significantly reduce the memory usage in the key-value gather and token-to-token attention process, as shown in Figure 4. In addition, we can reduce the overall amount of memory usage by approximately $5\times$.

4.5. Ablation Study

We conducted some ablation studies to prove that our SSCAN is more effective than other methods. All experiments were trained basically with top-k 32 and top-k 64 in inference on the scale of $\times 4$. Based on our findings, SSCAN pro-

Table 3. An ablation study of the order of Fine-grained Routing Attention and Window Attention.

Order	Set5	Set14	BSD100	Urban100
	PSNR / SSIM	PSNR / SSIM	PSNR / SSIM	PSNR / SSIM
Only <i>WA</i>	32.44 / 0.8976	28.77 / 0.7858	27.69 / 0.7406	26.47 / 0.798
<i>WA</i> \rightarrow <i>FGCA</i>	32.55 / 0.8987	28.874 / 0.7875	27.735 / 0.7421	26.626 / 0.8003
<i>FGCA</i> \rightarrow <i>WA</i>	32.576 / 0.8991	28.879 / 0.7878	27.735 / 0.7422	26.652 / 0.8021

Table 4. Ablation study of different window sizes at a scale factor of $\times 2/\times 3/\times 4$

Window Size	Top-k	Scale	Set14	BSD100	Urban100
			PSNR / SSIM	PSNR / SSIM	PSNR / SSIM
8 \times 8	64	X2	33.929 / 0.9211	32.326 / 0.9016	32.708 / 0.9337
4 \times 4	256		33.911 / 0.9200	32.322 / 0.9014	32.825 / 0.9342
8 \times 8	64	X3	30.610 / 0.8466	29.254 / 0.8095	28.740 / 0.8638
4 \times 4	256		30.592 / 0.8463	29.247 / 0.8089	28.804 / 0.8643
8 \times 8	64	X4	28.879 / 0.7878	27.735 / 0.7422	26.652 / 0.8021
4 \times 4	256		28.887 / 0.7878	27.739 / 0.7422	26.671 / 0.8027

vides guidelines for designing SISR model architectures.

Effectiveness of Top-k In Table 2, it can be observed that increasing the top-k value during the inference phase generally results in higher PSNR and SSIM values. This improvement is attributed to the ability to capture more relevant information. However, we observe that for some datasets, there are slight or no increase about some datasets. This phenomenon occurs because, for these datasets, lower top-k is already sufficient to capture the relevant key-value windows similar to the query. In the case of the Urban100 [19] dataset, which contains a significant amount of repetitive pattern information, there are numerous windows similar to the query so that higher top-k values enable the model to capture more relative information, resulting in notable improvements on PSNR and SSIM.

Analysis of Different Window Sizes To test the performance of fine-grained context-aware attention with varying window sizes, we train this model with window sizes of 4 and 8, and each top-k set to 256 and 64 for inference, so that the models can have the same amount of information. As shown in Table 4, at a scale factor of $\times 4$, the performance is slightly better at a window size of 4 than 8.

However, for scale factors $\times 2$ and $\times 3$, we find a performance drop when the window size is 4 for most datasets, but for the Urban100 [19] dataset, there is a significant performance increase of up to 0.12dB . Since the Urban100 [19] dataset has more repeated patterns than other datasets, our context-aware attention mechanism reconstructs more effectively. Also because the image size is larger than other datasets, our fixed window size technique allows it to capture more fine-grained information, where a large window size may unintentionally capture unrelated parts to the query, leading to a significant performance improvement over other datasets. This demonstrates the importance of adapting window strategies to the inherent characteristics

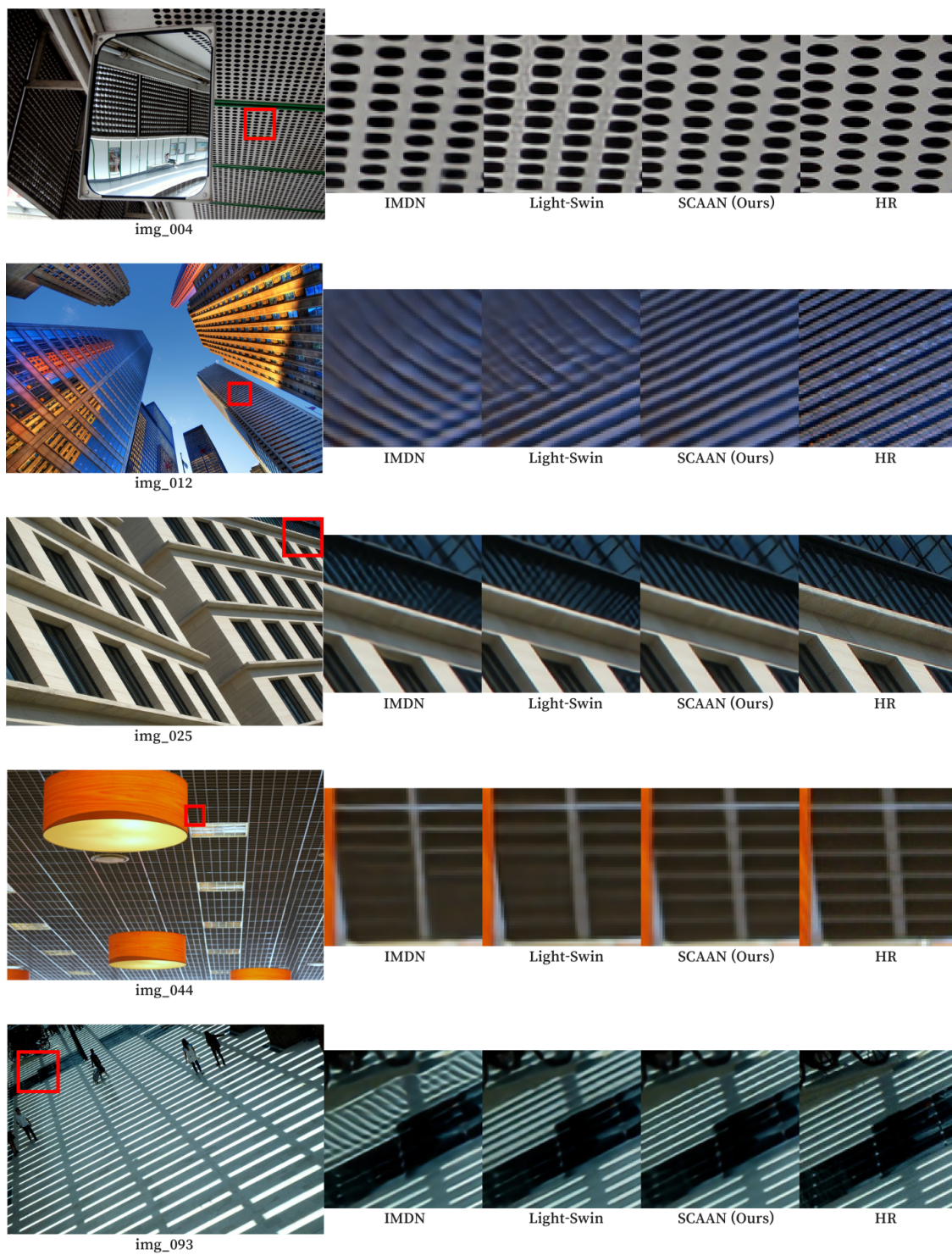


Figure 5. Visual comparisons of SSCAN with other publicly released SISR models on Urban100 dataset (×4).

of the data, especially in high-resolution settings.

Balance between Local and Global Feature To analyze the importance of integrating local and global features and their impact on feature extraction timing, we evaluate four different models, as shown in Table 3. First, Case 1 captures only local features and this cannot lead to performance improvement in the SISR tasks. Case 2 and Case 3, which incorporate both local and global attention, exhibit substantial performance gains, confirming that integrating both feature types is beneficial for SISR tasks.

To test where to use those global features for optimal performance in super-resolution, we designed two detailed configurations: Case 2, where fine-grained context-aware attention is placed before the WA layer, and Case 3, where fine-grained context-aware attention is applied after the WA layer. In Case 2, local features are extracted first, followed by global features. Conversely, in Case 3, global features are captured first, with local feature extraction occurring at the end of the block.

Experimental results indicate that a balanced integration of local and global features within a block yields the best SISR performance, rather than prioritizing one over the other. This suggests that maintaining a balanced representation of both feature types is crucial for achieving optimal results in super-resolution tasks.

4.6. Visual Results

We compare the visual quality of Urban100 [19] SISR results using our SCAAN compared with IMDN [20], SwinIR-light [28] on $\times 4$ upscaling task shown in Fig. 5. Transformer-based model Swin-light [28] is known for its performance in the state-of-the-art, but we can see that it still has some distortion for repeated pattern information in other images, which can also be observed worse in a CNN-based model IMDN [20].

In “img_004”, previous models show undesired artifacts such as ringing artifacts in the form of white bands around the black circle and failed to reconstruct the circle properly, while SSCAN reconstruct the circle well enough for the HR image. Also, they have suffered from distortion in “img_012” or reconstruction in the unintended direction of patterns in “img_025”. In contrast, Our SSCAN model reconstructs patterns straight and in the correct orientation, without distortion. There are many repeats of long and sharp patterns in “img_044” and “img_093”. Additionally, we also observe that previous models either recover it more boldly or blurry, but our SSCAN has the powerful ability to distinguish them as thin and clear ones. These comparisons indicate that SSCAN has a remarkable ability to recover visible details well.

5. Discussion on Future Work

In SSCAN, the choice of window size significantly impacts both computational efficiency and high-resolution reconstruction performance. Since the optimal window size may vary depending on the pixel distribution of each input image, an adaptive mechanism is needed to dynamically determine the most suitable window size. As part of our future research, we aim to develop a neural network-based framework that learns to adjust window sizes through fine-tuning on specific datasets, optimizing super-resolution quality accordingly. Additionally, in SSCAN, the top-k most relevant fine-grained context-aware attention windows are selected for attention computation. However, the optimal k values may also vary based on the image’s internal pixel distribution. In future work, we plan to explore a type of self-adaptive strategy to determine the optimal k dynamically, ensuring improved performance across diverse image distributions.

6. Conclusion

In this paper, we propose SSCAN, an acceptable framework that introduces query-adaptive context-aware attention to simultaneously capture both local and global features. Our method selects the top-k most similar key-value windows for each query, ensuring that only the most semantically relevant features contribute to reconstruction while preventing interference from irrelevant regions. To enhance efficiency in resource-constrained environments, we integrate (1) fixed-sized windows and (2) flash attention, enforcing linearity in token-to-token attention while significantly reducing memory usage. Moreover, SSCAN mitigates the quadratic growth in computation and memory consumption for large-scale images, making it more scalable than existing approaches. Extensive experiments demonstrate that SSCAN outperforms recent SISR models across multiple benchmark datasets, highlighting its effectiveness in high-quality super-resolution.

Acknowledgment

We would like to express our gratitude to Mr. Jason for his insightful feedback and discussions that facilitated this research. This research was carried out independently, without any external funding or financial support. Instead, we acknowledge the contributions of the open-source community, whose tools and datasets played a crucial role in this research.

References

- [1] Andreas Aakerberg, Kamal Nasrollahi, and Thomas B Moeslund. Real-world super-resolution of face-images from

- surveillance cameras. *IET Image Processing*, 16(2):442–452, 2022. 1
- [2] Eirikur Agustsson and Radu Timofte. Ntire 2017 challenge on single image super-resolution: Dataset and study. In *Proceedings of the IEEE conference on computer vision and pattern recognition workshops*, pages 126–135, 2017. 5, 6
- [3] Namhyuk Ahn, Byungkon Kang, and Kyung-Ah Sohn. Fast, accurate, and lightweight super-resolution with cascading residual network, 2018. 6
- [4] Saeed Anwar, Salman Khan, and Nick Barnes. A deep journey into super-resolution: A survey. *ACM Computing Surveys (CSUR)*, 53(3):1–34, 2020. 2
- [5] Mustafa Ayazoglu. Extremely lightweight quantization robust real-time single-image super resolution for mobile devices. In *Proceedings of the IEEE/CVF conference on computer vision and pattern recognition*, pages 2472–2479, 2021. 1
- [6] Marco Bevilacqua, Aline Roumy, Christine Guillemot, and Marie-Line Alberi-Morel. Low-complexity single-image super-resolution based on nonnegative neighbor embedding. In *British Machine Vision Conference, BMVC 2012, Surrey, UK, September 3-7, 2012*, pages 1–10. BMVA Press, 2012. 6
- [7] Anthony Cabrera, Seth Hitefield, Jungwon Kim, Seyong Lee, Narasinga Rao Miniskar, and Jeffrey S Vetter. Toward performance portable programming for heterogeneous systems on a chip: A case study with qualcomm snapdragon soc. In *2021 IEEE High Performance Extreme Computing Conference (HPEC)*, pages 1–7. IEEE, 2021. 1
- [8] Hanting Chen, Yunhe Wang, Tianyu Guo, Chang Xu, Yiping Deng, Zhenhua Liu, Siwei Ma, Chunjing Xu, Chao Xu, and Wen Gao. Pre-trained image processing transformer, 2021. 1
- [9] Xiangyu Chen, Xintao Wang, Jiantao Zhou, Yu Qiao, and Chao Dong. Activating more pixels in image super-resolution transformer. In *Proceedings of the IEEE/CVF Conference on Computer Vision and Pattern Recognition (CVPR)*, pages 22367–22377, 2023. 1, 3
- [10] Marcos V Conde, Eduard Zamfir, Radu Timofte, Daniel Motilla, Cen Liu, Zexin Zhang, Yunbo Peng, Yue Lin, Jiaming Guo, Xueyi Zou, et al. Efficient deep models for real-time 4k image super-resolution. ntire 2023 benchmark and report. In *Proceedings of the IEEE/CVF Conference on Computer Vision and Pattern Recognition*, pages 1495–1521, 2023. 1
- [11] Tri Dao, Daniel Y. Fu, Stefano Ermon, Atri Rudra, and Christopher Ré. Flashattention: Fast and memory-efficient exact attention with io-awareness, 2022. 7
- [12] Chao Dong, Chen Change Loy, Kaiming He, and Xiaoou Tang. Learning a deep convolutional network for image super-resolution. In *Computer Vision—ECCV 2014: 13th European Conference, Zurich, Switzerland, September 6-12, 2014, Proceedings, Part IV 13*, pages 184–199. Springer, 2014. 1, 2
- [13] Chao Dong, Chen Change Loy, and Xiaoou Tang. Accelerating the super-resolution convolutional neural network. In *Computer Vision—ECCV 2016: 14th European Conference, Amsterdam, The Netherlands, October 11-14, 2016, Proceedings, Part II 14*, pages 391–407. Springer, 2016. 1, 2
- [14] Xiaoyi Dong, Jianmin Bao, Dongdong Chen, Weiming Zhang, Nenghai Yu, Lu Yuan, Dong Chen, and Baining Guo. Cswin transformer: A general vision transformer backbone with cross-shaped windows. In *Proceedings of the IEEE/CVF conference on computer vision and pattern recognition*, pages 12124–12134, 2022. 1
- [15] Alexey Dosovitskiy, Lucas Beyer, Alexander Kolesnikov, Dirk Weissenborn, Xiaohua Zhai, Thomas Unterthiner, Mostafa Dehghani, Matthias Minderer, Georg Heigold, Sylvain Gelly, et al. An image is worth 16x16 words: Transformers for image recognition at scale. *arXiv preprint arXiv:2010.11929*, 2020. 1, 2
- [16] Lihua Fu, Hanxu Jiang, Huixian Wu, Shaoxing Yan, Junxiang Wang, and Dan Wang. Image super-resolution reconstruction based on instance spatial feature modulation and feedback mechanism. *Applied Intelligence*, 53(1):601–615, 2023. 1
- [17] Ganzorig Gankhuyag, Kihwan Yoon, Jinman Park, Haeng Seon Son, and Kyoungwon Min. Lightweight real-time image super-resolution network for 4k images. In *Proceedings of the IEEE/CVF Conference on Computer Vision and Pattern Recognition*, pages 1746–1755, 2023. 1
- [18] Yucheng Hang, Qingmin Liao, Wenming Yang, Yupeng Chen, and Jie Zhou. Attention cube network for image restoration. In *Proceedings of the 28th ACM International Conference on Multimedia*, pages 2562–2570, 2020. 6
- [19] Jia-Bin Huang, Abhishek Singh, and Narendra Ahuja. Single image super-resolution from transformed self-exemplars. In *Proceedings of the IEEE Conference on Computer Vision and Pattern Recognition*, pages 5197–5206, 2015. 6, 7, 9
- [20] Zheng Hui, Xinbo Gao, Yunchu Yang, and Xiumei Wang. Lightweight image super-resolution with information multi-distillation network. In *Proceedings of the 27th ACM International Conference on Multimedia (ACM MM)*, pages 2024–2032, 2019. 6, 9
- [21] Zheng Hui, Xinbo Gao, Yunchu Yang, and Xiumei Wang. Lightweight image super-resolution with information multi-distillation network. In *Proceedings of the 27th acm international conference on multimedia*, pages 2024–2032, 2019. 2
- [22] Diksha Khurana, Aditya Koli, Kiran Khatter, and Sukhdev Singh. Natural language processing: State of the art, current trends and challenges. *Multimedia tools and applications*, 82(3):3713–3744, 2023. 1
- [23] Jiwon Kim, Jung Kwon Lee, and Kyoung Mu Lee. Accurate image super-resolution using very deep convolutional networks. In *Proceedings of the IEEE conference on computer vision and pattern recognition*, pages 1646–1654, 2016. 1, 2
- [24] Furkan Kinli, Baris Ozcan, and Furkan Kirac. Instagram filter removal on fashionable images. In *Proceedings of the IEEE/CVF Conference on Computer Vision and Pattern Recognition*, pages 736–745, 2021. 1
- [25] Christian Ledig, Lucas Theis, Ferenc Huszár, Jose Caballero, Andrew Cunningham, Alejandro Acosta, Andrew Aitken, Alykhan Tejani, Johannes Totz, Zehan Wang, et al. Photo-

- realistic single image super-resolution using a generative adversarial network. In *Proceedings of the IEEE conference on computer vision and pattern recognition*, pages 4681–4690, 2017. 2
- [26] Royson Lee, Stylianos I Venieris, Lukasz Dudziak, Sourav Bhattacharya, and Nicholas D Lane. Mobisr: Efficient on-device super-resolution through heterogeneous mobile processors. In *The 25th annual international conference on mobile computing and networking*, pages 1–16, 2019. 1
- [27] Wenbo Li, Kun Zhou, Lu Qi, Nianjuan Jiang, Jiangbo Lu, and Jiaya Jia. Lapar: Linearly-assembled pixel-adaptive regression network for single image super-resolution and beyond, 2021. 6
- [28] Jingyun Liang, Jiezhong Cao, Guolei Sun, Kai Zhang, Luc Van Gool, and Radu Timofte. Swinir: Image restoration using swin transformer. In *Proceedings of the IEEE/CVF international conference on computer vision*, pages 1833–1844, 2021. 1, 5, 6, 9
- [29] Bee Lim, Sanghyun Son, Heewon Kim, Seungjun Nah, and Kyoung Mu Lee. Enhanced deep residual networks for single image super-resolution. In *Proceedings of the IEEE conference on computer vision and pattern recognition workshops*, pages 136–144, 2017. 1, 2
- [30] Jie Liu, Jie Tang, and Gangshan Wu. Residual feature distillation network for lightweight image super-resolution, 2020. 6
- [31] Xin Liu, Yang Li, Josh Fromm, Yuntao Wang, Ziheng Jiang, Alex Mariakakis, and Shwetak Patel. Splitsr: An end-to-end approach to super-resolution on mobile devices. *Proceedings of the ACM on Interactive, Mobile, Wearable and Ubiquitous Technologies*, 5(1):1–20, 2021. 1
- [32] Ze Liu, Yutong Lin, Yue Cao, Han Hu, Yixuan Wei, Zheng Zhang, Stephen Lin, and Baining Guo. Swin transformer: Hierarchical vision transformer using shifted windows. In *Proceedings of the IEEE/CVF international conference on computer vision*, pages 10012–10022, 2021. 1, 2
- [33] Xiaotong Luo, Yuan Xie, Yulun Zhang, Yanyun Qu, Cuihua Li, and Yun Fu. Latticenet: Towards lightweight image super-resolution with lattice block. In *Computer Vision–ECCV 2020: 16th European Conference, Glasgow, UK, August 23–28, 2020, Proceedings, Part XXII 16*, pages 272–289. Springer, 2020. 6
- [34] D. Martin, C. Fowlkes, D. Tal, and J. Malik. A database of human segmented natural images and its application to evaluating segmentation algorithms and measuring ecological statistics. In *Proceedings Eighth IEEE International Conference on Computer Vision. ICCV 2001*, pages 416–423 vol.2, 2001. 6
- [35] Liye Mei, Xinglong Hu, Zhaoyi Ye, Linfeng Tang, Ying Wang, Di Li, Yan Liu, Xin Hao, Cheng Lei, Chuan Xu, et al. Gtmfuse: Group-attention transformer-driven multi-scale dense feature-enhanced network for infrared and visible image fusion. *Knowledge-Based Systems*, 293:111658, 2024. 1
- [36] Yiqun Mei, Yuchen Fan, and Yuqian Zhou. Image super-resolution with non-local sparse attention. In *Proceedings of the IEEE/CVF Conference on Computer Vision and Pattern Recognition (CVPR)*, pages 3517–3526, 2021. 1
- [37] Harsh Nilesh Pathak, Xinxin Li, Shervin Minaee, and Brooke Cowan. Efficient super resolution for large-scale images using attentional gan. In *2018 IEEE International Conference on Big Data (Big Data)*, pages 1777–1786. IEEE, 2018. 1
- [38] Nathanaël Carraz Rakotonirina and Andry Rasoanaivo. Esrgan+: Further improving enhanced super-resolution generative adversarial network. In *ICASSP 2020-2020 IEEE International Conference on Acoustics, Speech and Signal Processing (ICASSP)*, pages 3637–3641. IEEE, 2020. 2
- [39] Shitao Tang, Jiahui Zhang, Siyu Zhu, and Ping Tan. Quadtree attention for vision transformers. *arXiv preprint arXiv:2201.02767*, 2022. 3
- [40] Chunwei Tian, Xuanyu Zhang, Jerry Chun-Wei Lin, Wangmeng Zuo, Yanning Zhang, and Chia-Wen Lin. Generative adversarial networks for image super-resolution: A survey. *arXiv preprint arXiv:2204.13620*, 2022. 1
- [41] Zhengzhong Tu, Hossein Talebi, Han Zhang, Feng Yang, Peyman Milanfar, Alan Bovik, and Yinxiao Li. Maxvit: Multi-axis vision transformer. In *European conference on computer vision*, pages 459–479. Springer, 2022. 1, 3
- [42] Ashish Vaswani, Noam Shazeer, Niki Parmar, Jakob Uszkoreit, Llion Jones, Aidan N Gomez, Łukasz Kaiser, and Illia Polosukhin. Attention is all you need. *Advances in neural information processing systems*, 30, 2017. 1, 2
- [43] Chaofeng Wang, Zhen Li, and Jun Shi. Lightweight image super-resolution with adaptive weighted learning network. *arXiv preprint arXiv:1904.02358*, 2019. 6
- [44] Wenxiao Wang, Wei Chen, Qibo Qiu, Long Chen, Boxi Wu, Binbin Lin, Xiaofei He, and Wei Liu. Crossformer++: A versatile vision transformer hinging on cross-scale attention, 2023. 1
- [45] Xintao Wang, Ke Yu, Shixiang Wu, Jinjin Gu, Yihao Liu, Chao Dong, Yu Qiao, and Chen Change Loy. Esrgan: Enhanced super-resolution generative adversarial networks. In *Proceedings of the European conference on computer vision (ECCV) workshops*, pages 0–0, 2018. 1, 2
- [46] Xuehui Wang, Qing Wang, Yuzhi Zhao, Junchi Yan, Lei Fan, and Long Chen. Lightweight single-image super-resolution network with attentive auxiliary feature learning, 2020. 6
- [47] Yulin Wang, Rui Huang, Shiji Song, Zeyi Huang, and Gao Huang. Not all images are worth 16x16 words: Dynamic transformers for efficient image recognition. *Advances in neural information processing systems*, 34:11960–11973, 2021. 3
- [48] Yutong Xie, Jianpeng Zhang, Yong Xia, Anton van den Hengel, and Qi Wu. Clustr: Exploring efficient self-attention via clustering for vision transformers. *arXiv preprint arXiv:2208.13138*, 2022. 3
- [49] Yiran Xu, Taesung Park, Richard Zhang, Yang Zhou, Eli Shechtman, Feng Liu, Jia-Bin Huang, and Difan Liu. Videogigagan: Towards detail-rich video super-resolution. *arXiv preprint arXiv:2404.12388*, 2024. 1
- [50] Jianwei Yang, Chunyuan Li, Pengchuan Zhang, Xiyang Dai, Bin Xiao, Lu Yuan, and Jianfeng Gao. Focal self-attention for local-global interactions in vision transformers. *arXiv preprint arXiv:2107.00641*, 2021. 3

- [51] Roman Zeyde, Michael Elad, and Matan Protter. On single image scale-up using sparse-representations. In *Curves and Surfaces*, pages 711–730, Berlin, Heidelberg, 2012. Springer Berlin Heidelberg. [6](#)
- [52] Dafeng Zhang, Feiyu Huang, Shizhuo Liu, Xiaobing Wang, and Zhezhu Jin. Swinir: Revisiting the swinir with fast fourier convolution and improved training for image super-resolution. *arXiv preprint arXiv:2208.11247*, 2022. [5](#)
- [53] Tianyi Zhang, Kishore Kasichainula, Yaoxin Zhuo, Baoxin Li, Jae-Sun Seo, and Yu Cao. Transformer-based selective super-resolution for efficient image refinement. In *Proceedings of the AAAI Conference on Artificial Intelligence*, pages 7305–7313, 2024. [1](#)
- [54] Xindong Zhang, Hui Zeng, Shi Guo, and Lei Zhang. Efficient long-range attention network for image super-resolution, 2022. [6](#)
- [55] Lei Zhu, Xinjiang Wang, Zhanghan Ke, Wayne Zhang, and Rynson WH Lau. Biformer: Vision transformer with bi-level routing attention. In *Proceedings of the IEEE/CVF Conference on Computer Vision and Pattern Recognition*, pages 10323–10333, 2023. [1](#), [3](#), [5](#), [7](#)